A Decentralized and Communication-free Control Algorithm of DC Microgrids for the Electrification of Rural Africa

Lucas Richard[1,2], David Frey[1], Marie-Cécile Alvarez-Herault[1], Bertrand Raison[1]
[1]Univ. Grenoble Alpes, CNRS, Grenoble INP*, G2Elab, France
[2]Nanoé, France
Email: lucas.richard@g2elab.grenoble-inp.fr

Keywords

≪Smart microgrids≫, ≪Nanogrid≫, ≪Renewable energy systems≫, ≪Test bench≫, ≪Decentralized control structure≫, ≪DC-DC converter≫, ≪Control methods for electrical systems≫

Abstract

Following the United Nation Sustainable Development Goals of ensuring universal access to basic and modern electric services by 2030, a strong research interest has emerged in the power grid community to design microgrids adapted for rural electrification of Sub-Saharan countries. Their optimal topology, their stability as well as their control architecture are still open to debate. However, DC microgrids with decentralized storage and production are increasingly gaining attention as they enable the progressive building of electric infrastructure in a bottom-up manner, which increases the economic viability, the modularity and the scalability of such rural electrification scheme. In addition, there is a growing consensus in terms of control for decentralized and communication-free algorithms. The absence of a centralized controller is crucial to avoid a single point of failure and to enable plug & play feature within the microgrid. Moreover, DC microgrids must be robust and affordably deployable even in areas with limited or no telecommunication signals. Therefore, this paper proposes the design through software simulations of a decentralized and communication-free control algorithm of DC microgrids adapted for the rural electrification of Africa. The proposed control is then thoroughly validated on a lab test bench and extensive results are presented.

Introduction

Rural electrification is one of the biggest challenges that Sub-Saharan Africa and South-East Asia are facing nowadays to improve living conditions of millions and foster socio-economic development [1, 2, 3]. Indeed, despite the United Nation (UN) goals of ensuring universal access to basic and modern clean energy services by 2030 [4], almost one billion people are still lacking access to electricity, trapping them in energy poverty [5]. The vast majority of unelectrified people reside in rural places of Sub-Saharan Africa or South-East Asia, where abundant resources of solar energy are available [5, 6].
In the past decade, DC microgrids have gained attention as a promising solution to tackle rural electrification problematics [1, 2, 3, 6, 7]. Unlike Solar Home Systems (SHS), microgrids offer the possibilities of building medium-scale power grids, allowing productive use of energy, without necessarily the huge investment costs needed for national grid extension. However, their optimal topology, sizing and control architecture remain unanswered questions open to debates [8, 9]. Centralized power architectures have recently been widely installed whereas decentralized topologies have shown lower upfront costs and better efficiency than centralized ones [2, 10]. In addition, decentralized architectures enable the progressive building of electric infrastructures in a bottom-up manner, growing with the needs of the communities [6]. This also breaks down large initial investment costs in successive small parts, increasing the economic sustainability of rural electrification projects. This is therefore the belief of the authors that DC microgrids with decentralized production and storage is preferable, as advocated by the swarm

*Institute of Engineering Univ. Grenoble Alpes

electrification concept [3]. For instance, such DC microgrids can be build on already installed SHS or nanogrids (NG), i.e. a solar panel, a lead-acid battery for 4 to 6 households as installed by Nanoé, a French-Malagasy social venture, in Madagascar [6].
However, such DC microgrids are entirely based on power electronic converters. The topology of DC microgrids as well as their operation and cost-effectiveness are unavoidably intertwined with their control algorithm. To avoid a single point of failure where any problem would impact the whole microgrid and to enable plug & play feature on the microgrid, centralized controllers are less and less favored, even if they facilitate the proper operation of the DC microgrids. Therefore, there is a strong research interest on distributed [11, 12] and fully decentralized control algorithms [10, 13, 14, 15, 16, 17, 18, 19]. However, distributed control schemes always require communication between adjacent controllers, which dramatically reduces the economic viability of the proposed solution while increasing its technical complexity. For those reasons, distributed schemes are often put aside for rural electrification projects.
Most research works propose State-of-Charge (SoC) based droop control for DC microgrids with decentralized production and storage, but they either implement voltage droop control (V-I droop) [16, 17, 18] or current droop control (I-V droop) [10, 13, 14, 15]. However, I-V droop control offers faster dynamics in comparison to V-I droop and only necessitate the setting of one PI regulator [10]. The objectives of the proposed control algorithms vary, from SoC equalizing or balancing between the batteries distributed over the microgrids to communal load supporting. All research papers design and validate their proposed control algorithm through software simulation but only [10, 13, 14, 15, 19] (at the Center for Research on Microgrids (CROM) facilities and at the University of Manitoba) carry out experimental validation.
Based on those observations, this paper proposes a decentralized and communication-free control algorithm to interconnect NGs with the objective to form a village-wide DC microgrid. This control algorithm is adapted for the progressive building of electric infrastructures designed for rural Sub-Saharan Africa and is validated through software simulations and a lab test bench.

Solar DC Microgrid for Swarm Electrification

Microgrid Topology

The microgrid under study is shown in Fig. 1. This microgrid is designed to interconnect 12 or 24 V NGs installed by Nanoé in Madagascar and composed of one solar panel (between 150 and 300 W), one lead acid battery (between 90 Ah and 260 Ah) for 4 to 6 houses [6]. The NGs are usually 20 to 80 meters away from each other within a village and would be connected through 16 or 25 mm^2 electric lines. The NGs are interconnected to a 60 V DC bus through bidirectional DC-DC buck-boost converters.

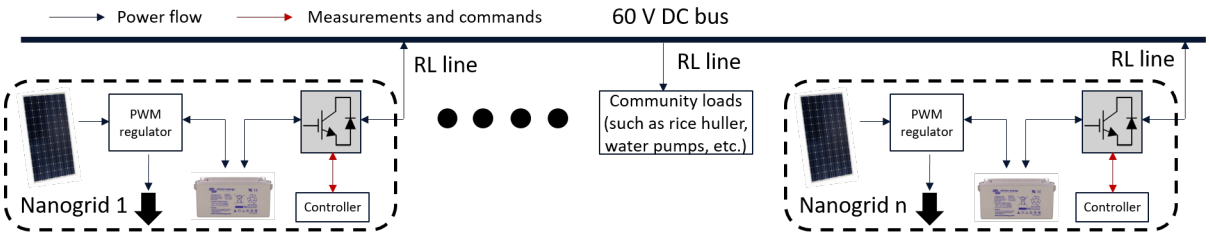

Fig. 1: Topology of the proposed microgrid.

The objectives of forming a village-wide microgrid are twofold. Firstly, by mutualizing installed production and storage capacities, the hardware resources will be used more efficiently, improving the economic and environmental sustainability of those rural electrification projects. Secondly, such DC microgrids will increase the electrical services brought to the communities through enhanced reliability and high-power communal loads (e.g. agro-processing machines, water pumps, etc.), enabling the end-users to progressively climb the energy ladder. Such communal loads can be connected directly to the 60 V DC bus or through a DC-DC converter depending on their nature.

Decentralized and Communication-free Control Algorithm

The proposed topology implies that the control algorithm of the microgrid is decentralized to avoid a single point of failure and enable plug & play feature and communication-free to be affordably deployable even in areas where telecommunication signals are inexistent or unreliable. The plug & play feature is of particular importance for the swarm electrification approach as the basic power units (e.g. NGs, SHS) are supposed to be able to operate in full autonomy and must then be able to connect and disconnect from the microgrid without any impact on the rest of the microgrid. In addition, even if a microgrid is already deployed, new power units could be installed and later connected to the microgrid.

Due to its decentralized nature, the control algorithm can only rely on local variables. Therefore, the control algorithm must pilot energy sharing (i.e. the magnitude of current injection or absorption) based on the DC bus voltage, representing the global level of available energy on the microgrid, and on the SoC of the NG battery, indicating the level of local available energy. The higher the DC voltage, the more globally charged is the microgrid and vice versa. High and low limits (arbitrarily set at $\pm$ 10%) are imposed on the DC bus voltage so that the control algorithm enables relevant power flows while guarantying stability and maintaining the DC bus voltage within a pre-defined zone. This relationship between the DC bus voltage level and the global level of energy on the microgrid is crucial for further expansion of the electric infrastructure (e.g. microgrid interconnection or connection to an AC grid). In addition, three levels of battery SoC are defined, weak from 0 to 60% SoC, medium for 60 to 80% SoC and strong for above 80% SoC. The control algorithm must ensure that any NG with a higher SoC range supports the other NGs with a lower SoC range, with respect to their respective energy reserve. The control algorithm, inspired by [10] with additional modifications on the mode equations, defines different modes of current injection or absorption depending on the DC bus voltage and the local SoC, as shown in Fig. 2 and described below. Table I summarises the different parameters of the control algorithm, whose values have been tuned through software simulations and could easily be modified if necessary.

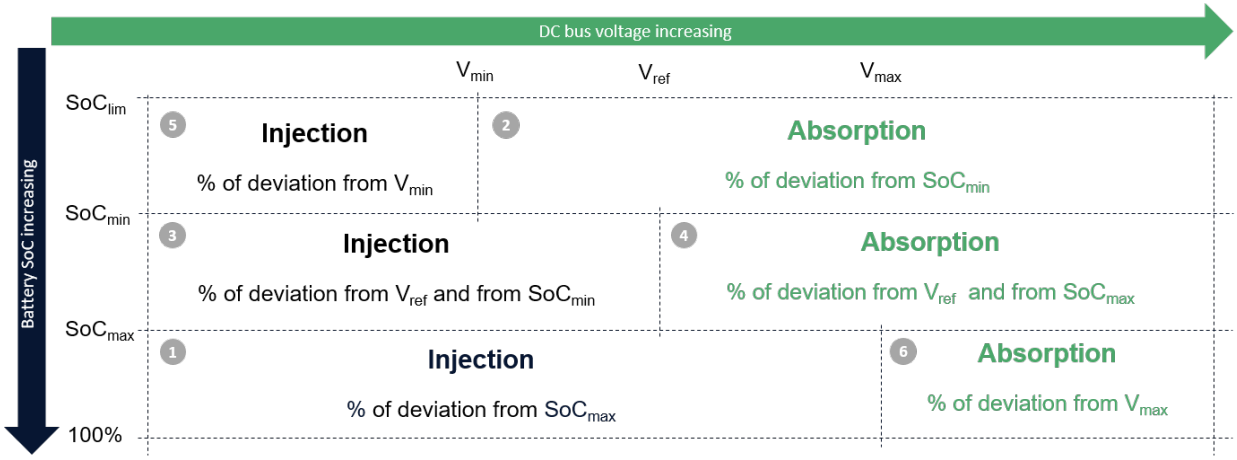

Fig. 2: Decentralized and communication-free control algorithm.

1. Pure Injection

The NG is strong with a SoC above 80% whereas, within the microgrid, some NGs can absorb current, as the DC bus voltage is below V_{max}. The NG therefore injects current with respect to its own SoC, and the higher the SoC, the greater the current injected. A limit is set on the maximum injected current with I_{rated} equal to $C_{bat}/10$. The α exponent enables faster power sharing by increasing the current reference value at a given SoC in comparison with a linear evolution. Lastly, to avoid any edge or pumping effect when the control algorithm suddenly changes mode or is blocked around a DC bus voltage at the boundary of two modes (or around a SoC value for modes 3 and 4), the current reference function is made continuous with respect to the DC bus voltage through the introduction of hyperbolic tangents.

$$I_{ref} = I_{rated} \cdot \left(\frac{SoC - SoC_{max}}{1 - SoC_{max}} \right)^{\alpha} \cdot \tanh\left(\gamma_v \cdot (V_{max} - V_{bus}) \right) \tag{1}$$

2. Pure Absorption
On the opposite to Pure injection, the NG is weak with a SoC below 60% whereas, within the microgrid, some NGs can inject current, as the DC bus voltage is above V_{min}. The NG therefore absorbs current with respect to its SoC, and the lower the SoC, the greater the current absorbed. A limit is set on the maximum absorbed current at I_{rated} at a SoC equal or below SoC_{lim}. The roles of α and of the hyperbolic tangent are similar than in the Pure Injection mode.

$$I_{ref} = max\left(-I_{rated}, -I_{rated} \cdot \left(\frac{SoC - SoC_{min}}{SoC_{lim} - SoC_{min}} \right)^{\alpha} \cdot \tanh\left(\gamma_v \cdot (V_{bus} - V_{min}) \right) \right) \tag{2}$$

3. Voltage-controlled Injection
The NG is in the medium zone with its SoC between SoC_{min} and SoC_{max} and the microgrid is globally discharged as indicated by a DC bus voltage below V_{ref}. Therefore, the NG injects current with a SoC-based droop control with an injected current proportional to the DC bus voltage deviation to V_{ref}. The droop coefficient varies between $1/R_d$ at SoC_{min} and $2/R_d$ at SoC_{max} so that the higher the SoC, the greater the current injected to the microgrid. The maximal current injected is also limited to I_{rated}. An additional coefficient $\frac{C_{bat}}{C_{max}}$ is included to take into account the battery capacity so that the higher the battery capacity, the greater the current injected. For similar reasons to modes 1 and 2, hyperbolic tangents are introduced to make the current reference function continuous with respect to the SoC.

$$\begin{cases} k_d = \frac{1}{R_d} \cdot \left(1 + \frac{SoC - SoC_{min}}{SoC_{max} - SoC_{min}} \right) \cdot \tanh\left(\gamma_s \cdot (SoC_{max} - SoC) \right) \cdot \tanh\left(\gamma_s \cdot (SoC - SoC_{min}) \right) \\ I_{ref} = min\left(I_{rated}, k_d \cdot \frac{C_{bat}}{C_{max}} \cdot (V_{ref} - V_{bus}) \right) \end{cases} \tag{3}$$

4. Voltage-controlled Absorption
The NG is in the medium zone with its SoC between SoC_{min} and SoC_{max} and the microgrid is globally charged as indicated by a DC bus voltage above V_{ref}. Therefore, the NG absorbs current with a SoC-based droop control with an absorbed current proportional to the DC bus voltage deviation to V_{ref}. The droop coefficient varies between $2/R_d$ at SoC_{min} and $1/R_d$ at SoC_{max} so that the lower the SoC, the greater the current absorbed from the microgrid. In a similar fashion to the Voltage-controlled Injection, a current limit, a coefficient $\frac{C_{bat}}{C_{max}}$ and hyperbolic tangents are introduced.

$$\begin{cases} k_c = \frac{1}{R_d} \cdot \left(2 - \frac{SoC - SoC_{min}}{SoC_{max} - SoC_{min}} \right) \cdot \tanh\left(\gamma_s \cdot (SoC_{max} - SoC) \right) \cdot \tanh\left(\gamma_s \cdot (SoC - SoC_{min}) \right) \\ I_{ref} = max\left(-I_{rated}, k_c \cdot \frac{C_{bat}}{C_{max}} \cdot (V_{ref} - V_{bus}) \right) \end{cases} \tag{4}$$

5. Voltage-regulated Injection
The NG is in the weak zone with a SoC below SoC_{min} as well as the rest of the microgrid, as indicated by a voltage below V_{min}. Therefore, the NG must support the DC bus voltage to bring it back to V_{min} through a voltage-droop control with a V_{min} setpoint. A limit at I_{rated} is set. This Voltage-regulated Injection mode is counter-intuitive as a weak NG must inject to the microgrid but is necessary to maintain the microgrid on and to guarantee that the DC bus voltage stays within a pre-defined zone (between V_{min} and V_{max}). However, the NGs should rarely be in this mode or at least they should be between Mode 2 and 5 with a DC bus voltage settled at V_{min} (with I_{ref} then at 0 A), indicating an overall weak microgrid.

$$I_{ref} = min\left(I_{rated}, \frac{V_{min} - V_{bus}}{R_d} \right) \tag{5}$$

6. Voltage-regulated Absorption
The NG is in the strong zone with a SoC above SoC_{max} as well as the rest of the microgrid, as indicated by a voltage above V_{max}. Therefore, the NG must support the DC bus voltage to bring it back to V_{max} through a voltage-droop control with a V_{max} setpoint. A limit at I_{rated} is set. This Voltage-regulated Absorption

mode is counter-intuitive as a strong NG must absorb current from the NG but is necessary to guarantee the DC bus voltage stays within a pre-defined zone (between V_{min} and V_{max}). However, the NGs should rarely be in this mode or at least they should be between Mode 1 and 6 with a DC bus voltage settled at V_{max} (with I_{ref} then at 0 A), indicating an overall strong microgrid.

$$I_{ref} = max\left(-I_{rated}, \frac{V_{max} - V_{bus}}{R_d} \right) \tag{6}$$

Table I: Parameters of the control algorithm.

Parameters	V_{ref}	V_{min}	V_{max}	SoC_{max}	SoC_{min}	SoC_{lim}	R_d	α	γ_v	γ_s	C_{bat}	C_{max}	I_{rated}
Value	60 V	54 V	66 V	80%	60%	30%	0.5	1/3	5	50	Capacity of the NG	180 Ah	$\frac{C_{bat}}{10}$

A selfish behavior can also be added to the control algorithm to favor self-recharging before supporting the other NGs in the medium zone, by staying a longer time in mode 3 or 4. To this end, SoC_{max} can be first set at 95%. Then, once the SoC of the NG has reached 95% (i.e. self-recharging can be considered almost complete), SoC_{max} is changed to 80% to fully support the other NGs by shifting to mode 1. However, this selfish behavior still enables the support of the weak NGs through modes 3 and 4.

Software Validation

High-level Simulation Model

A simulation model of the microgrid is needed to validate and tune the proposed control algorithm. A microgrid interconnecting 5 NGs is modelled in Matlab-Simulink, with averaged models for the converters [20] to enable long-term simulation of a few days of operation in a few minutes. Each NG is fully modelled with PV production, household consumption and lead-acid battery storage. Then, each NG is connected to the 60 V DC bus through a current-controlled bidirectional buck-boost converter whose current reference is given by the control algorithm presented in the previous section. Field data from Nanoé [6] are used for the geographical layout of the microgrid, shown in Fig. 3, and for the NGs consumption and production. The SoC of each NG battery is evolving according to its local production/consumption balance and its exchange with the microgrid. The resistances of the power lines are taken into account with a resistance per km of 1.465 Ω/km (i.e. for 25 mm aluminium cable). A communal load can be included within the simulation with an adjustable power consumption. In addition, this model can easily be extended to a higher number of NGs or communal loads.

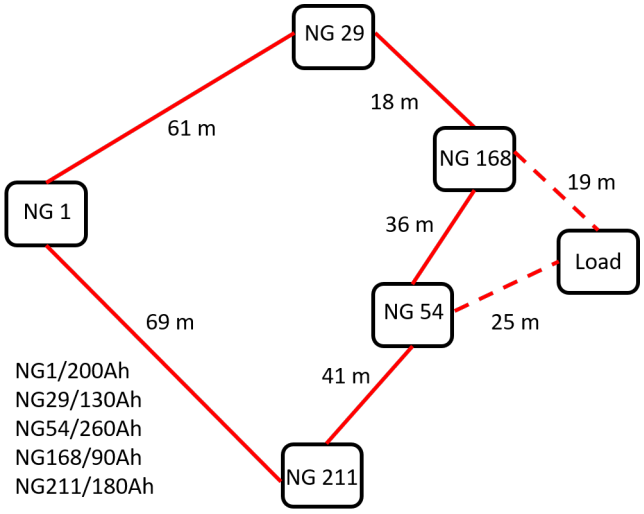

Fig. 3: Topology of the simulated microgrid.

Software Results

Fig. 4 and Fig. 5 show the evolution of the current exchanged between the NGs, of the DC bus voltage and of the SoC of each NG with and without a microgrid for more than 3 days of operation. For illustration purposes, the consumption of NGs 29 and 168 (from Nanoé field data [6]) have been doubled, which makes them undersized, and the simulation is started with unusually low SoC at 3:40 pm. The selfish feature of the control algorithm is enabled. Note that a positive current is injected on the microgrid and vice versa. It can be seen that NGs 1, 54 and 211 support most of the time NGs 29 and 168, either in Voltage-controlled mode 3 or 4 or in Pure Injection mode 1, depending on their SoC level. In addition, the DC bus voltage does traduce well the overall energy availability on the microgrid. Most importantly, Fig. 5 proves that interconnecting NGs enables to supply an overall higher load demand than with isolated NGs. Without the microgrid, to support a twice bigger demand, NGs 29 and 168 would need a bigger installation. The microgrid enables to optimise the use of hardware resources of the NGs already installed, both to allow for higher electrical services and to enhance the economic sustainability of the proposed rural electrification scheme.

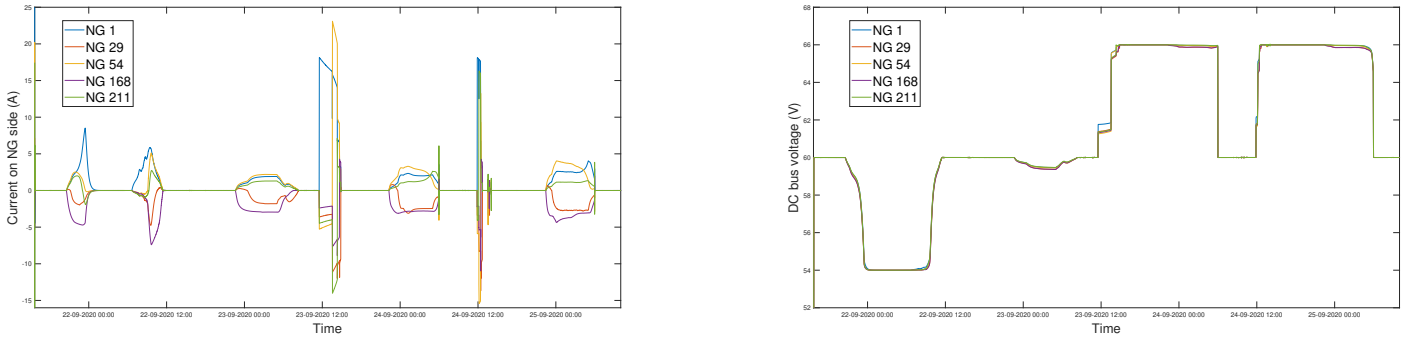

Fig. 4: Long-term current exchange and DC bus voltage evolution.

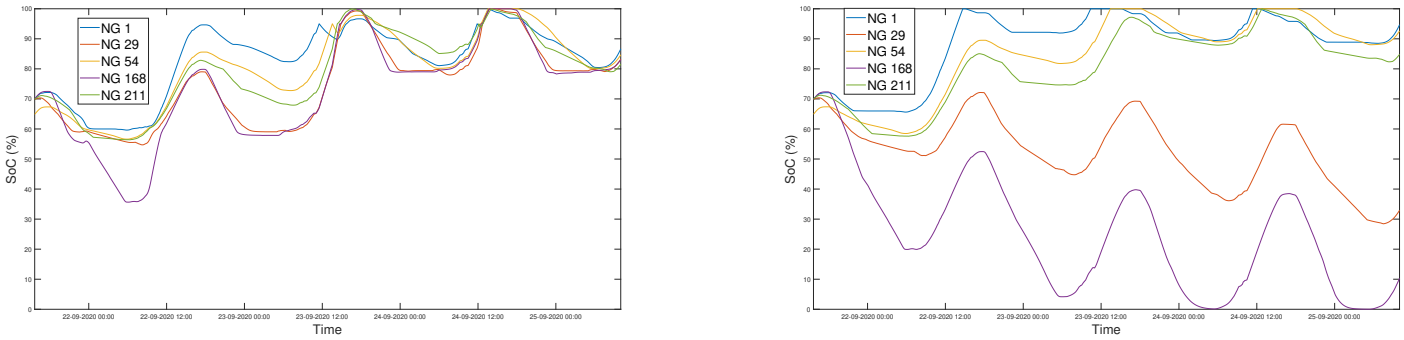

Fig. 5: Long-term State-of-Charge evolution with (left figure) and without a microgrid (right figure).

The different modes of the control algorithm are illustrated in Fig. 6 and Fig. 7, where the SoC of each NG is artificially changed within the simulation, to illustrate different operating points. At t=0 s, NG 1 is strong with a SoC at 100%, NGs 29, 54 and 168 are in the medium zone with SoCs respectively at 70%, 75% and 65%, and NG 211 is weak with a SoC at 40%. Therefore, NG 1 is in Pure Injection Mode, NG 29, 54 and 168 are in Voltage-controlled Absorption Mode whereas NG 211 is in Pure Absorption Mode. However, as the DC bus voltage is close to 60 V, NG 29, 54 and 168 do not absorb much current. From t=1000 s, as the SoC of NG 211 starts to increase, NG 211 switches to Voltage-controlled Absorption from t=1400 s to t=2200 s, then to Pure Injection Mode. Note than NG 1 is then injecting more current on the microgrid than NG 211 due to its greater battery capacity. Similarly, NG 54 is absorbing more current from t=1400 to t=2800 s than NG 29 and 168. As the SoC of NG 54, 168 and 29 start to increase respectively at t=2500 s, t=3500 s and t=4500 s, the NGs switch modes from Voltage-controlled Absorption modes to Pure Injection. Once all the NG have reached the strong zone, the DC bus voltage stabilizes at 66 V, as the NGs are at the equilibrium between the Pure Injection Mode and the Voltage-regulated absorption to keep the DC bus voltage within its pre-defined zone. It can be noted than due

to the voltage drops on the lines, the closer a strong NG is from a weak NG, the more current it will inject on the DC bus as it sees a more accurate image of the DC bus voltage. The farther a NG is from a consumption point, the higher the voltage drop, and the less accurate is the DC bus voltage with respect to the consumption point.

In addition, the proposed DC microgrid enables to power communal loads by all the NGs, with respect to their respective SoC and to their proximity to the communal load. Fig. 8 illustrates the operation of the microgrid with a communal load. All the NGs are strong with their SoC at 100%. At t=1000 s, a 300 W load is connected to the DC bus and it is respectively increased to 600 and 900 W at t=2500 s and t=4000 s, then disconnected at t=5500 s. The communal load is installed close to NG 54 and 168, as shown in Fig. 3. Therefore, NG 54 and 168 are injecting the most current on the microgrid with respect to their battery capacity, respectively 260 Ah and 90 Ah. On the opposite, NG 1, the second strongest NG on the microgrid is injecting very little current to power the communal load as it is located far away from it. This can also be seen with the DC bus voltage witnessed by NG 1 and NG 211, which are significantly greater than the DC bus voltage witnessed by the other NGs. Thus, due to the voltage drops on the lines, NG 1 and 211 do not know there is a high power demand on the microgrid. This shows that the geographical dissemination of strong and weak NGs as well as of communal loads must be carefully planned to obtain a balanced microgrid.

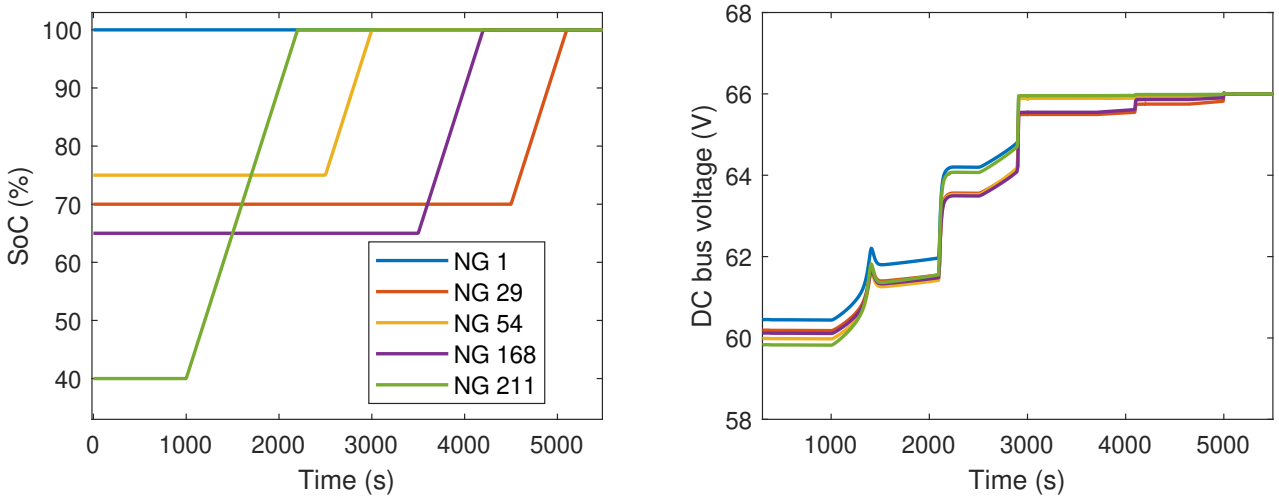

Fig. 6: Different SoC and DC bus voltage operating points.

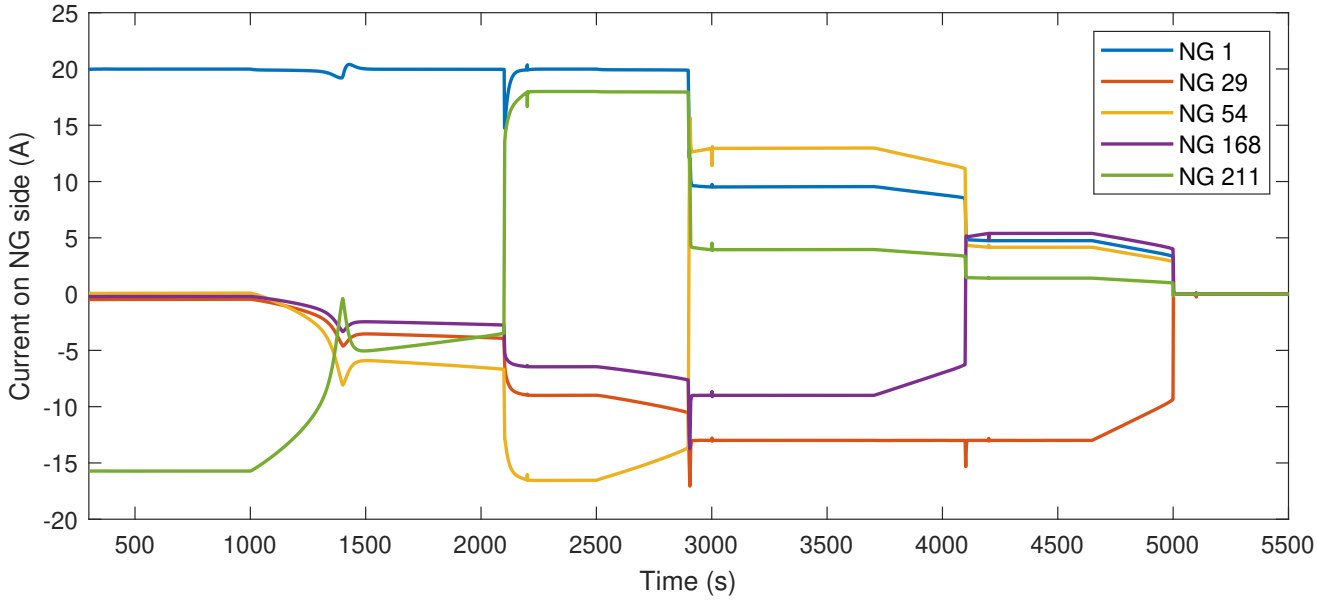

Fig. 7: Current exchanged between the nanogrids at different operating points.

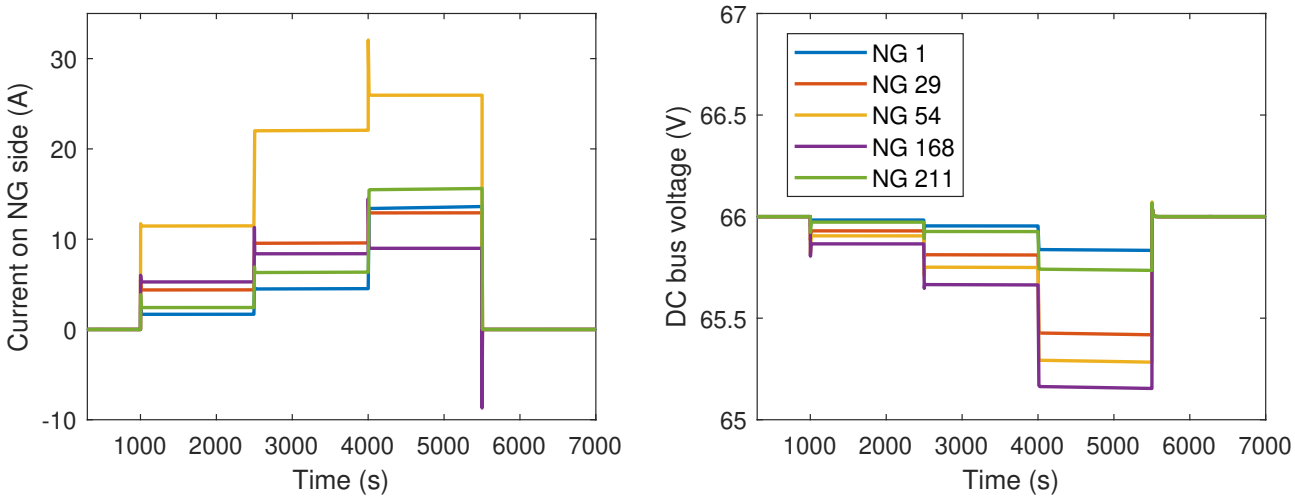

Fig. 8: Communal load operation.

Experimental Validation

Lab Test Bench

A test bench has been developed in the lab to experimentally validate and further tune the proposed control algorithm. The test bench contains 3 bidirectional buck-boost converters developed in-house, interconnected through RL lines emulating the impedances of the electric lines on the field. At the input of each converter, a power supply in parallel to an electronic load or a battery is connected. Each converter is controlled by a MyRio Embedded Controller, from National Instruments, programmed in LabVIEW [21]. The MyRio controller associated with LabVIEW enables to implement the proposed control algorithm, to emulate a SoC estimator (and associated scenario of SoC evolution), to record data every 25 ms and to ease monitoring through a Graphic User Interface (GUI). A communal load, emulated by a power resistor, can be connected to the DC bus. In addition, grid reconfiguration is easily doable in order to test different grid topologies (i.e. radial or meshed). Fig. 9 shows the schematic of the lab test bench and its actual set-up.

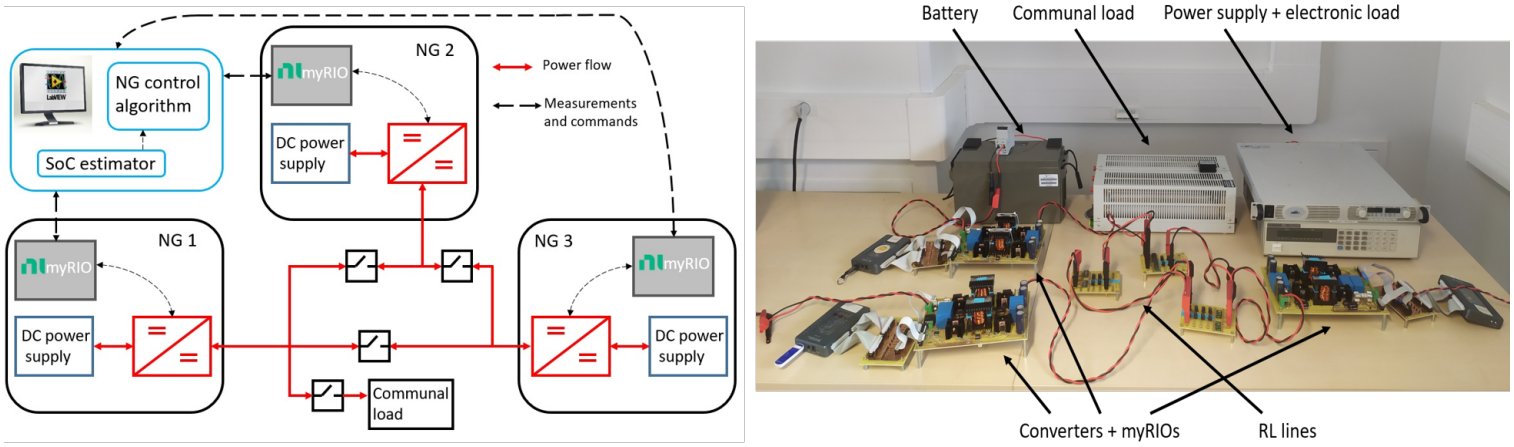

Fig. 9: Schematic and actual set-up of the DC microgrid test bench.

Experimental Results

The test bench permits complete monitoring of the power flows on the DC microgrid, tuning of the control algorithm parameters and extensive testing of its capabilities. Fig. 10 a) shows the evolution of the DC bus voltage and the current exchanged between the 3 converters (named NG 1, NG 2 and NG 3) at different operating points. The SoCs are artificially changed within the LabVIEW GUI to replicate

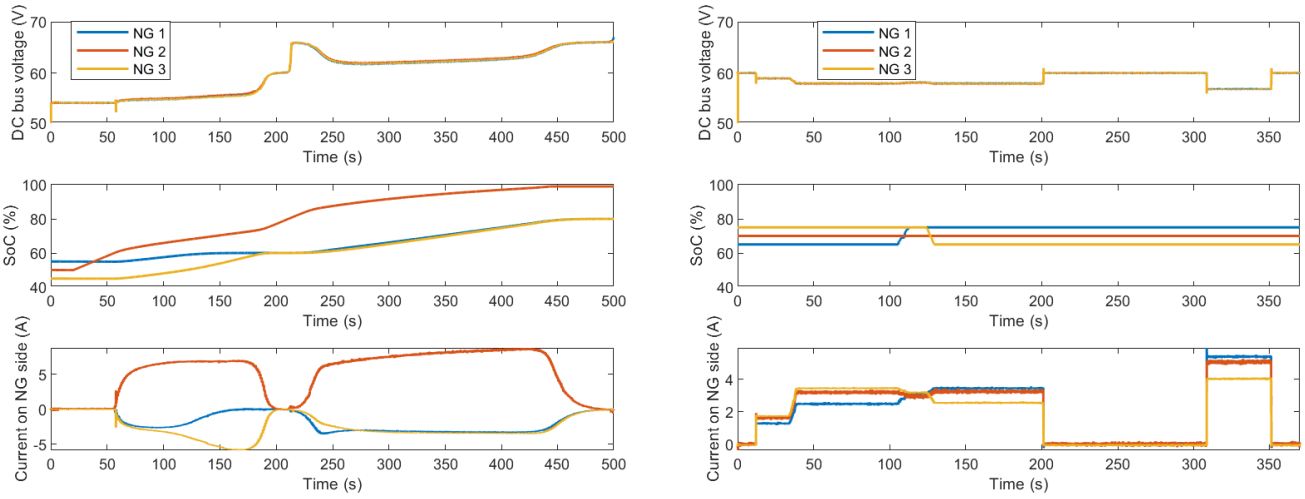

Fig. 10: (a) Experimental results at different operating points, (b) with communal load operation.

a potential real SoC evolution within a short time frame. The 3 NGs are initialized in the weak zone (i.e. SoC<60%), therefore they are operating in Voltage-regulated Mode, stabilizing the DC bus voltage at 54 V. As the SoC of NG 2 reaches 60%, NG 2 starts to operate in Voltage-controlled Mode and, the DC bus voltage being low, it injects current on the DC bus that NG 1 and NG 3 absorb, being now in Pure Absorption Mode. At t=180 s, the 3 NGs are in the medium zone, therefore the DC bus voltage is maintained at 60 V. Once NG 2 reaches a SoC above 80%, it switches to Pure Injection Mode and injects current on the DC bus. As a response to the increase of the DC bus voltage, NG 1 and 3, in Voltage-controlled Mode, absorb currents until their SoC reaches 80%. Note that here the selfish behavior of the control is not implemented and that I_{rated} is equal to 9 A.

Furthermore, Fig. 10 b) illustrates the operation of a communal load on the DC microgrid. The SoC of each NG is initialized in the medium zone. At t=10 s, the power resistor is connected to the DC bus with low power consumption, which is increased at t=30 s. The NGs are in Voltage-controlled Mode and therefore respond to the DC bus voltage deviation to V_{ref}, i.e. 60 V, by injecting current to the DC bus, with respect to their own SoC. Within the medium zone, the higher the SoC, the higher the current injected (with some limitations when approaching 80% SoC due to the hyperbolic tangents). The load is then disconnected at t=200 s and reconnected at a greater power at t=310 s until t=350 s, to observe different operating points. At t=120 s, the SoCs are artificially changed to illustrate the current sharing scheme. Note here that the current injected by NG 2 is higher than the others with respect to its SoC due to is close proximity to the communal load. A zoom on the DC bus voltage indicates that NG 2 sees a DC bus voltage 0.1 to 0.15 V lower than NG 1 and 3, and thus injects more on the DC bus. Those results validate the operation of the microgrid with a communal load and confirm the importance of carefully selecting the location of a high-power communal load, as the neighbouring NGs will be the ones contributing the most.

Those experimental results have enabled to further tune the control algorithm. In particular, the slope of the voltage hyperbolic tangent (i.e. γ_v) has been decreased to avoid oscillations on the current reference, which should not evolve too fast. This illustrates the crucial need to confront theoretical control algorithms to the reality of test benches. Furthermore, additional studies can be easily performed on this test bench (e.g. different grid topologies and DC bus voltage levels, start-up and protection schemes [22]).

Conclusion

This paper presents a decentralized and communication-free control algorithm for DC microgrids adapted to the progressive building of electric infrastructures in rural Sub-Saharan Africa. The control algorithm is first designed through simulations and then experimentally validated and tuned on a test bench developed in-house.

Future works will focus on the enhancement of the control algorithm to include the control of the solar panel production to optimise the power flows within the NG and the charging of the NG battery. In addition, designing a reliable and precise SoC estimator is not straightforward, therefore, it would be of interest to study control algorithms based on the battery voltage instead of the SoC. Thus, accurate battery modelling is needed. Lastly, the impact of each local control algorithm on the overall stability of the DC microgrid should be thoroughly analysed.

References

[1] Moner-Girona, M., Bódis, K., Morrissey, J., Kougias, I., Hankins, M., Huld, T., Szabó, S. (2019). Decentralized rural electrification in Kenya: Speeding up universal energy access. Energy for Sustainable Development, Vol. 52, pp. 128–146.

[2] Nasir, M., Khan, H. A., Zaffar, N. A., Vasquez, J. C., Guerrero, J. M. (2018). Scalable Solar DC microgrids: On the Path to Revolutionizing the Electrification Architecture of Developing Communities. IEEE Electrification Magazine, Vol. 6, No. 4, pp. 63–72.

[3] Groh, S., Philipp, D., Lasch, B. E., Kirchhoff, H. (2015). Swarm Electrification: Investigating a Paradigm Shift Through the Building of Microgrids Bottom-up. Chapter 1 of Decentralized Solutions for Developing Economies, pp. 25-44.

[4] "United Nation 17 Sustainable Development Goals." (2022), [Online]. Available: https://sdgs.un.org/goals.

[5] "World Energy Outlook (WEO)." (2021), [Online]. Available: https://www.iea.org/reports/world-energy-outlook-2021.

[6] "Nanoé presentation website" (2022), [Online]. Available: https://www.nanoe.net/en/

[7] Jhunjhunwala, A., Lolla, A., Kaur, P. (2016). Solar-DC Microgrid for Indian Homes: A Transforming Power Scenario. IEEE Electrification Magazine, Vol. 4, No. 2, pp. 10–19.

[8] Dragicevic, T., Lu, X. Vasquez, J.C., Guerrero, J. M. (2016). DC Microgrids — Part I : A Review of Control Strategies and Stabilization Techniques. IEEE Transactions on Power Electronics, Vol. 31, No. 7, pp. 4876–4891.

[9] Meng, L., Shafiee, Q., Trecate, G. F., Karimi, H., Fulwani, D., Lu, X., Guerrero, J. M. (2017). Review on Control of DC Microgrids and Multiple Microgrid Clusters. IEEE Journal of Emerging and Selected Topics in Power Electronics, Vol. 5, No. 3, pp. 928–948.

[10] Nasir, M., Jin, Z., Khan, H. A., Zaffar, N. A., Vasquez, J. C., Guerrero, J. M. (2019). A Decentralized Control Architecture Applied to DC Nanogrid Clusters for Rural Electrification in Developing Regions. IEEE Transactions on Power Electronics, Vol. 34, No. 2, pp. 1773–1785.

[11] Shafiee, Q., Dragicevic, T., Andrade, F., Vasquez, J. C., Guerrero, J. M. (2014). Distributed consensus-based control of multiple DC-microgrids clusters. IECON Proceedings, pp. 2056–2062.

[12] Shafiee, Q., Dragičević, T., Vasquez, J. C., Guerrero, J. M. (2014). Hierarchical Control for Multiple DC-Microgrids Clusters. IEEE Transactions on Energy Conversion, Vol. 29, No. 4, pp. 922–933.

[13] Nasir, M., Anees, M., Khan, H. A., Guerrero, J. M. (2019). Dual-loop control strategy applied to the cluster of multiple nanogrids for rural electrification applications. IET Smart Grid, Vol. 2, No. 3, pp. 327–335.

[14] Li, D., Ho, C. N. M. (2021). A Module-Based Plug-n-Play DC Microgrid with Fully Decentralized Control for IEEE Empower a Billion Lives Competition. IEEE Transactions on Power Electronics, Vol. 36, No. 2, pp. 1764–1776.

[15] Nasir, M., Anees, M., Khan, H. A., Khan, I., Xu, Y., Guerrero, J. M. (2019). Integration and Decentralized Control of Standalone Solar Home Systems for Off-Grid Community Applications. IEEE Transactions on Industry Applications, Vol. 55, No. 6, pp. 7240–7250.

[16] Samende, C., Bhagavathy, S. M., McCulloch, M. (2019). State of Charge Based Droop Control for Coordinated Power Exchange in Low Voltage DC Nanogrids. Proceedings of the International Conference on Power Electronics and Drive Systems, July 2019.

[17] Samende, C., Bhagavathy, S. mothilal, Gao, F., McCulloch, M. (2021). Decentralized Voltage Control for Efficient Power Exchange in Interconnected DC Clusters. IEEE Transactions on Sustainable Energy, Vol 12, No. 1, pp 103-115.

[18] Lu, X., Sun, K., Guerrero, J. M., Vasquez, J. C., Huang, L. (2015). Double-Quadrant State-of-Charge-Based Droop Control Method for Distributed Energy Storage Systems in Autonomous DC Microgrids. IEEE Transactions on Smart Grid, Vol. 6, No. 1, pp. 147–157.

[19] Nasir, M., Khan, H. A., Hussain, A., Mateen, L., Zaffar, N. A. (2018). Solar PV-Based Scalable DC Microgrid for Rural Electrification in Developing Regions. IEEE Transactions on Sustainable Energy, Vol. 9, No. 1, pp. 390–399.

[20] "Average-Value chopper (Mathworks help)." (2022), [Online]. Available: https://fr.mathworks./help/physmod/sps/ref/averagevaluechopper.html.

[21] "LabVIEW presentation website." (2022), [Online].Available: https://www.ni.com/en-za/shop/labview.html.

[22] Richard, L., Derbey, A., Frey, D., Alvarez-Hérault, M.C., Raison, B. (2022) Experimental Design of Solar DC Microgrid for the Rural Electrification of Africa. In Proceedings of the PCIM Europe 2022, pp. 1–10